Enhancement of information transmission of sub-threshold signals applied to distal positions of dendritic trees in hippocampal CA1 neuron models with stochastic resonance

Article *in* Biological Cybernetics · September 2010

DOI: 10.1007/s00422-010-0395-5 · Source: PubMed

2 authors, including:

Dominique M Durand
Case Western Reserve University
270 PUBLICATIONS **6,313** CITATIONS

Biol Cybern (2010) 103:227–236
DOI 10.1007/s00422-010-0395-5

ORIGINAL PAPER

Biological Cybernetics

Enhancement of information transmission of sub-threshold signals applied to distal positions of dendritic trees in hippocampal CA1 neuron models with stochastic resonance

Hiroyuki Mino · Dominique M. Durand

Received: 28 September 2009 / Accepted: 28 May 2010 / Published online: 16 June 2010

Abstract Stochastic resonance (SR) has been shown to enhance the signal-to-noise ratio and detection of low level signals in neurons. It is not yet clear how this effect of SR plays an important role in the information processing of neural networks. The objective of this article is to test the hypothesis that information transmission can be enhanced with SR when sub-threshold signals are applied to distal positions of the dendrites of hippocampal CA1 neuron models. In the computer simulation, random sub-threshold signals were presented repeatedly to a distal position of the main apical branch, while the homogeneous Poisson shot noise was applied as a background noise to the mid-point of a basal dendrite in the CA1 neuron model consisting of the soma with one sodium, one calcium, and five potassium channels. From spike firing times recorded at the soma, the mutual information and information rate of the spike trains were estimated. The simulation results obtained showed a typical resonance curve of SR, and that as the activity (intensity) of sub-threshold signals increased, the maximum value of the information rate tended to increased and eventually SR disappeared. It is concluded that SR can play a key role in enhancing the information transmission of sub-threshold stimuli applied to distal positions on the dendritic trees.

Keywords Computer simulation · Poisson shot noise · Hodgkin–Huxley model · Information rate

H. Mino (✉)
Department of Electrical and Computer Engineering, Kanto Gakuin University, 1-50-1 Mutsuura E., Kanazawa-ku, Yokohama 236-8501, Japan
e-mail: mino@ieee.org

D. M. Durand
Department of Biomedical Engineering, Neural Engineering Center, Case Western Reserve University, 10900 Euclid Ave., Cleveland, OH 44106-7207, USA

1 Introduction

Stochastic resonance (SR) is a phenomenon that involves coupling between deterministic and random dynamics in non-linear systems (Gammaitoni et al. 1998). This phenomenon can be interpreted as an improved detection of low-level input signals when the noise level in the non-linear system increases. The phenomenon was observed first in climate dynamics (Benzi et al. 1981; Nicolis 1982), and since then, it has been demonstrated in a variety of systems (Moss et al. 1994; Simonotto et al. 1997; Moss 2000). SR has been observed in both peripheral nervous systems (Bulsara et al. 1991; Collins et al. 1996; Douglass et al. 1993; Moss et al. 2004) and central nervous systems (Stacey and Durand 2000, 2001, 2002). In every case, it was shown that the detection of a sub-threshold input signal was improved when a certain level of noise was added. Several review articles regarding the importance of "noise," variability, or fluctuations in neural information processing have been published (e.g., Stein et al. 2005; Destexhe et al. 2003).

In the study of SR, the signal-to-noise ratio (SNR) has played an important role, because SR is evaluated by a specific relationship between SNR and the noise intensity. The theoretical curve of SR can be expressed in terms of SNR, e.g., for monostable solution (Gammaitoni et al. 1998), as:

$$SNR \propto \left(\frac{\xi \Delta U}{D}\right)^2 e^{-(\Delta U/D)} \tag{1}$$

in which ξ, ΔU, and D denote the signal strength, the threshold barrier height, and the noise intensity, respectively. The expression indicates a resonant peak corresponding to the level of noise intensity that produces maximal SNR. In cases of a "periodic" sub-threshold stimulus, the SNR can be computed by taking a ratio of the signal power of the power spectrum at a specific frequency to that of noise. However,

this definition of SNR cannot be used to evaluate "aperiodic" or "random" signals, such as those in neuronal spikes, that carry information in real nervous systems. We also note that SNR could not tell us anything about the information rate of the data (Kish et al. 2001).

Information theory (Shannon 1949) has provided a framework for investigating information transmission via a communication channel with a measure of the mutual information, $I(X, Y)$, between the input signal (X) and output signal (Y):

$$I(X, Y) = H(Y) - H(Y|X), \tag{2}$$

where $H(Y)$ and $H(Y|X)$ stand for the entropy of Y and the conditional entropy of Y given X, respectively. This information-theoretic approach is useful to evaluate SR even with a random sub-threshold input signal (Bulsara and Zador 1996) and an output signal characterized by a sequence of spikes, "spike trains." In general, it would be difficult to compute the mutual information since the calculation requires knowledge of the joint probability density function of all possible signals and the resulting spike trains. However, if the inter-spike intervals (ISIs) of neuronal spikes are independent, i.e., renewal process (Cox and Lewis 1966; Snyder and Miller 1991), then the probability density function of a single ISI can be utilized for calculating the entropies (Bulsara and Zador 1996; Zador 1998), making it possible to reduce the computational difficulties.

Hippocampal CA1 neurons have a large apical dendritic trees (<500 μm in length) that receives thousands of synaptic inputs. Spruston et al. (1993) has suggested that synaptic inputs located at distal positions on the tree can attenuate to a level where they cannot have any significant summative effects on the soma, because of the large size of the trees and electrotonic distances. Although it was proposed in Magee and Johnston (1995) and Cook and Johnston (1997) that active channels in the dendrites could be responsible for amplifying the distal signals, SR can enhance detection of distal synaptic inputs in the presence of noise at physiological noise level (Stacey and Durand 2000). However, it is important for the analysis of signal processing in neuron to determine the effect of SR on information transmission between sub-threshold distal dendritic inputs and axonal output firing.

Therefore, the objective of this article is to test, through computer simulation, the hypothesis that information transmission of a random sub-threshold synaptic currents (signal) applied to a distal position of "passive dendritic trees" can be enhanced by optimally adding a homogeneous Poisson shot noise (background noise). Hippocampal CA1 neurons were represented by a multi-compartment model with synaptic input currents applied at different locations along the main apical branch in the CA1 neuron model, and the background noise applied as the sum of all background synaptic noise to the mid-point of a basal dendrite. The transmembrane potentials were recorded at the soma in the CA1 neuron model to obtain the information rate estimated from the total and noise entropies of the inter-spike interval histogram (ISIH) (Deco and Schumann 1997). The effect of the activity (intensity) and input location of sub-threshold synaptic currents on the information transmission through CA1 neuron models was investigated.

2 Methods

The hippocampal CA1 neuron was represented by a multi-compartment model (Traub 1982) with 26 compartments: 5 compartments in the basal tree, 1 compartment in the soma, and 20 compartments in the apical branches, as shown in Fig. 1. The dendritic model parameters were set as follows: basal dendrite diameter 4 μm, basal tree length 250 μm, soma diameter 15 μm, soma length 20 μm, apical diameter 3.5 μm, apical length 400 μm, auxiliary apical diameter 3.13 μm, auxiliary apical length 400 μm, main apical diameter 1 μm, and the main apical length 400 μm. The membrane specific resistance and capacitance in the dendrites were set at 14,000 Ω cm^2 and 2 μF/cm^2, while those in the soma were set at 28,000 Ω cm^2 and 1 μF/cm^2. All model parameters were adopted from those in (Stacey and Durand 2000). The soma contained one sodium, one calcium, and five potassium channels in which conductances, and transition rates were adopted from those in (Warman and Durand 1994). Although dendrites contain active conductances, experiments, and models with passive dendrites produced similar results (Stacey and Durand, 2000, 2001) suggesting that the effect is retained with simpler passive models. Therefore, a model of no active conductance in dendrites was adopted. The transmembrane potentials were numerically calculated by solving a diffusive partial differential equation with the Crank–Nicholson method at a sampling step of 20 μs (See Appendix).

For the computer simulations, the random synaptic input current (signal), $I_{\text{signal}_A}(t)$ (supra-threshold), $I_{\text{signal}_B}(t)$ (sub-threshold), or $I_{\text{signal}_C}(t)$ (sub-threshold), and "synaptic noise" current, $I_{\text{noise}}(t)$, of 30 s in time length were applied separately in each simulation to the main apical section (proximal, middle, or distal position), and the basal section, respectively, as shown in the top of Fig. 1, while the transmembrane potential at the soma, $V_{\text{soma}}(t)$, was recorded. The random synaptic current was assumed to be a homogeneous Poisson process filtered by an impulse response function as follows:

$$I_{\text{signal}}(t) = \int_{-\infty}^{t} h_{\text{signal}}(\tau) \mathrm{d}N_s(t - \tau) \tag{3}$$

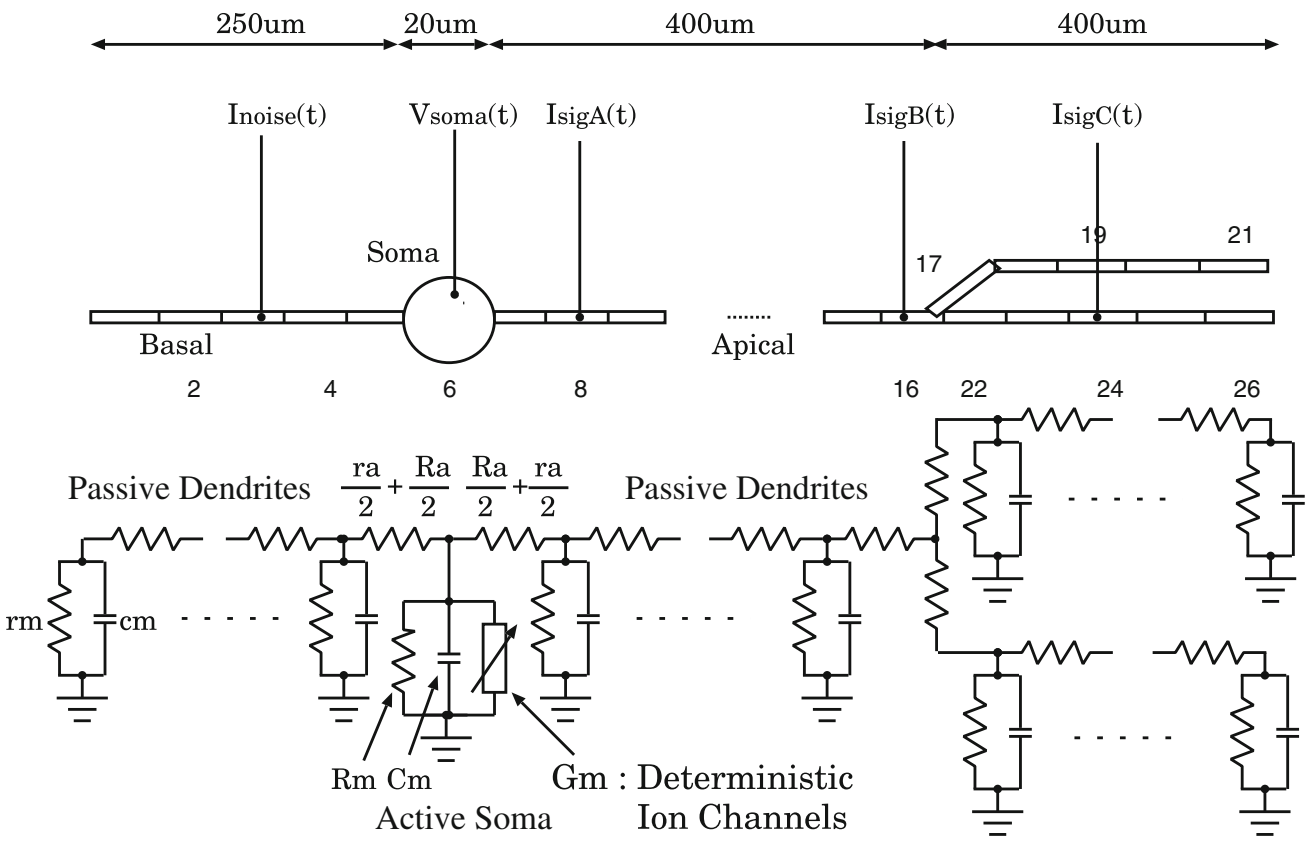

Fig. 1 Hippocampal CA1 neuron was represented as a 5 cylinder multi-compartment model possessing 26 compartments: 5 compartments in the basal, 1 compartment in the soma, and 20 compartments in the apical branches. The length in each segment was set at 250 μm in the basal, 10 μm in the soma, and 400 μm in apical, respectively, while the diameter was set at 4 μm (basal), 15 μm (soma), 3.5 μm (1° apical), 3.13 μm (*Auxiliary*2° apical), and 1 μm(Main 2° apical). The equivalent electric circuit is shown with the dendrites as passive networks and with the soma modeled with active channels. The "random synaptic current," $I_{\text{signal}_A}(t)$, $I_{\text{signal}_B}(t)$, or $I_{\text{signal}_C}(t)$, and "synaptic noise" current, $I_{\text{noise}}(t)$, were assumed to be applied to the main apical section (the 8th (proximal), 16th (middle), or 24th (distal) compartment), and the basal section (the 3rd compartment), respectively, while the transmembrane potential at the soma, $V_{\text{soma}}(t)$ was recorded

in which the intensity, λ, of the counting process $N_s(t)$ was set at 2.5, 5, 8, and 10 s^{-1}, and

$$h_{\text{signal}}(t) = a_{\text{signal}} e^{-\alpha_{\text{signal}} t} \quad (t \geq 0) \tag{4}$$

in which $a_{\text{signal}} = 1.1$ nA, and $\alpha_{\text{signal}} = 1000\ \text{s}^{-1}$. The signal amplitude was set to be sub-threshold for the middle and distal positions (B and C), but supra-threshold for the proximal position (A). The "background noise" current was generated to represent the sum of the noise sources distributed over dendritic trees by a homogeneous Poisson process filtered by the impulse response function as follows:

$$I_{\text{noise}}(t) = \int_{-\infty}^{t} h_{\text{noise}}(\tau) \mathrm{d}N_n(t-\tau) \tag{5}$$

in which the intensity of the counting process $N_n(t)$ was set at 100 s^{-1}, and

$$h_{\text{noise}}(t) = a_{\text{noise}} e^{-\alpha_{\text{noise}} t} \quad (t \geq 0) \tag{6}$$

where $\alpha_{\text{noise}} = 1000\,\text{s}^{-1}$, and a_{noise} denotes the amplitude of the impulse response function. a_{noise} was varied to determine the background noise on spike signal transmission. Ten different input waveforms were generated for each input waveform to obtain statistics (noise entropy). Typical examples of input, noise, and output waveforms generated by this model are shown in Fig. 2a. In addition, the relationship between the noise variance at soma without input signals and the amplitude of the background noise a_{noise} is plotted in Fig. 2b to verify that the noise in this model was within physiological level, i.e., 100–300 times of the baseline variance of 12,000 μV^2 observed in slice experiments (Stacey and Durand 2000). The mean (DC offset) of $I_{\text{noise}}(t)$ was estimated to be 0.0159 nA, while the mean (DC offset) of $V_m(t)$ was inferred as 0.5771 mV. The spike firings were not observed when a DC offset of 0.0159 nA was applied to the basal dendrite, i.e., $I_{\text{noise}}(t) = 0.0159$ nA. It follows from those results that the variation of $I_{\text{noise}}(t)$ creates the SR phenomena in this situation, and that the effects of the DC offset was negligible to the SR phenomena.

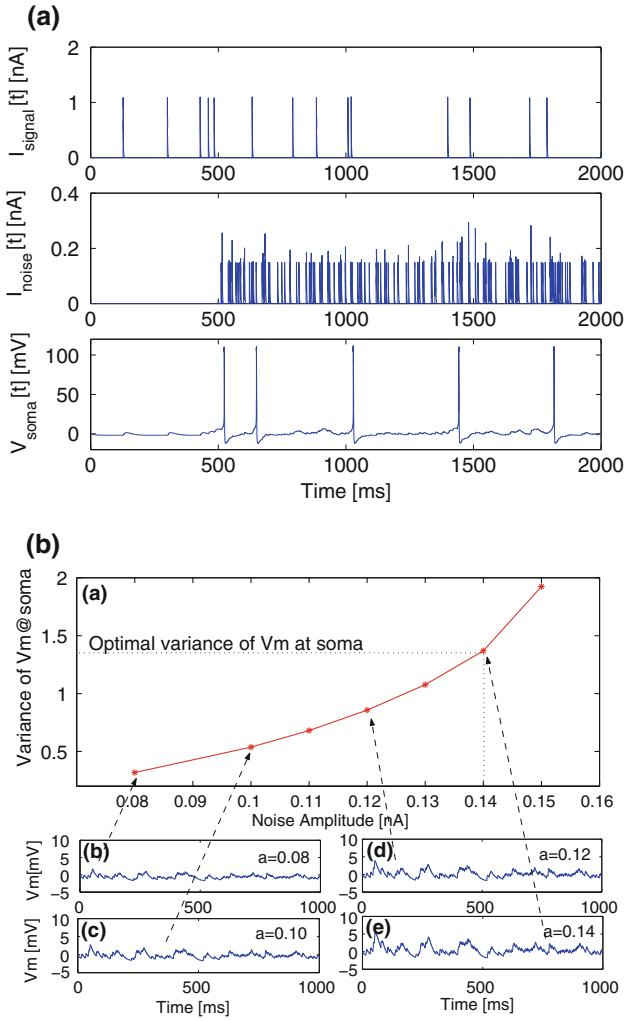

Fig. 2 **a** *Top* Sub-threshold current applied to the distal point, $I_{\text{signal}_C}(t)$, a Poisson shot noise with an intensity of 5 s^{-1} in which $a_{\text{signal}} = 1.1$ nA. *Middle* Background noise, $I_{\text{noise}}(t)$, a Poisson shot noise with an intensity of 100 s^{-1} in which a_{noise}, was set at 0.15 nA. *Bottom* Transmembrane potentials at soma, $V_{\text{soma}}(t)$, relative to the resting potential. Note that the background noise induces the spike firings after 500 ms. **b** Variance of the transmembrane potential V_m, relative to the resting potential, at soma in mV^2 versus the amplitude of the background noise a_{noise} in nA

A spike firing was defined as a local maximum of the transmembrane potential if it exceeded half the peak value of an average action potential. The inter-spike interval (ISI) histogram, the post-stimulus time (PST) histogram, and the raster plot were generated from spike firing times where the bin width of the ISI histogram, bw, was determined by evaluating the following formula (Scott 1979):

$$bw = 3.49 \times \sigma_{\text{ISI}} \times N_{\text{ISI}} \tag{7}$$

where σ_{ISI} and N_{ISI} are the standard deviation and the number of the ISI data, respectively. From those histograms the information rate bits/s was calculated, assuming that the ISIs were independent, i.e., renewal point process, (de Ruyter van Steveninck et al. 1997; Rieke et al. 1997; Bulsara and Zador 1996; Zador 1998; Dayan and Abbott 2001; Brette and Guigon 2003):

$$I_{\text{rate}}(I_{\text{signal}}(t), T) = R[H_{\text{total}}(T) - H_{\text{noise}}(T|I_{\text{signal}}(t))] \tag{8}$$

where

$$H_{\text{total}}(T) = -\sum_{i=0}^{\infty} p(T_i) \log_2 p(T_i) \tag{9}$$

and

$$H_{\text{noise}}(T|I_{\text{signal}}(t)) = -E\left[\sum_{i=0}^{\infty} p(T_i|I_{\text{signal}}(t)) \log_2 p(T_i|I_{\text{signal}}(t))\right] \tag{10}$$

in which T and R are the ISIs, and the rate of output spike firings, respectively, E[] denotes the expectation operation. In practical situations, E[] was performed by taking an ensemble average of ten sample realizations.

Computer simulations were performed on an IBM compatible PC with an Intel Core 2 Quad Q6600 CPU. The computer codes were written in JAVA, while the graphics were depicted with MATLAB.

3 Results

3.1 Effect of background noise on information rate

To determine the effect of the background noise on the information transmission of sub-threshold signals, both noise and signal were applied to the CA1 neuron model. A random sub-threshold synaptic current $I_{\text{signal}_C}(t)$ was applied to distal dendric location C (see Fig. 1) with an intensity of 5 s^{-1} and an impulse response function of $h_{\text{signal}}(t) = a_{\text{signal}} \exp(-1000t)$, where $a_{\text{signal}} = 1.1$ nA (top of Fig. 3a–c). The background noise, $I_{\text{noise}}(t)$, was a homogeneous Poisson shot noise with an intensity of 100 s^{-1} and an impulse response function of $h_{\text{noise}}(t) = a_{\text{noise}} \exp(-1000t)$ (2nd row of Fig. 3a–c), the raster plots of 30 trials (3rd row of Fig. 3a–c), and the post-stimulus time histogram (PSTH) (bottom of Fig. 3a–c). To determine the relationship between the input and output, raster plots and PSTH were generated at various noise amplitude $a_{\text{noise}}(t) = 0.1$, 0.15, and 0.3 nA in Fig. 3a–c. The raster plots (3rd row) and the PSTH (bottom) in Fig. 3 show that the random sub-threshold synaptic currents were encoded with a higher reliability into the spike firings, when a_{noise} increased from 0.1 to 0.15 nA (a, b), but decreased when the noise increased to 0.3 nA (c).

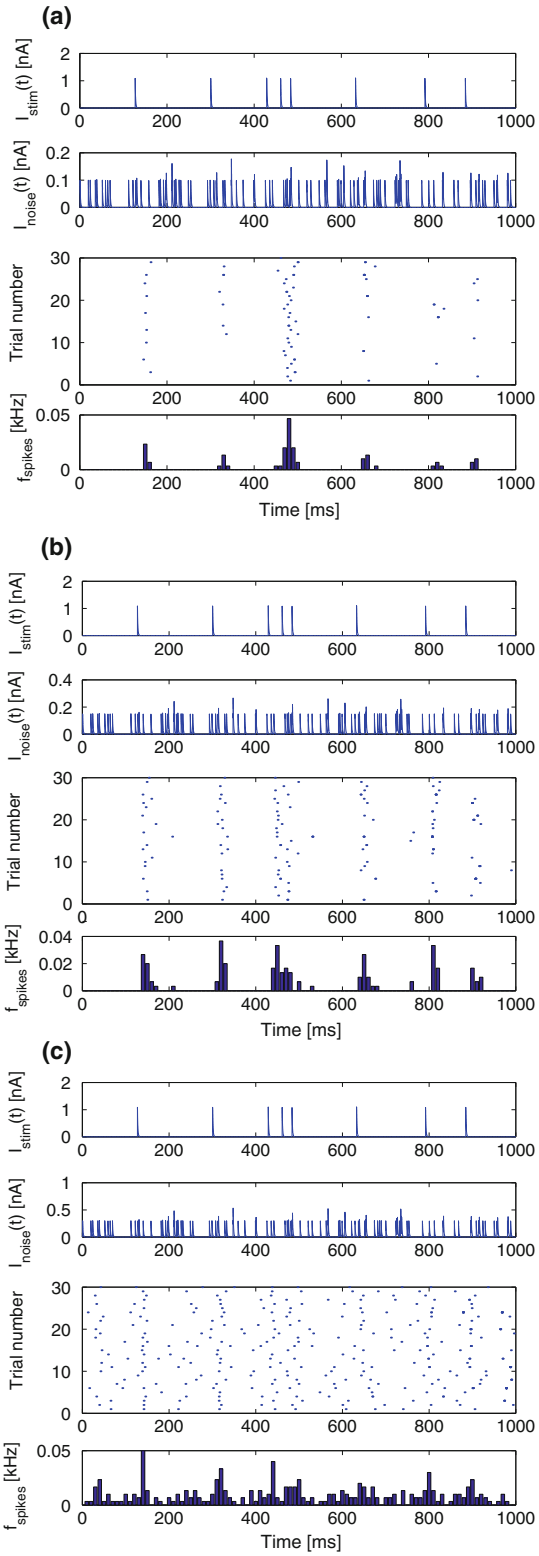

Fig. 3 *Top* Sub-threshold current applied to the distal point, $I_{\text{signal}_C}(t)$, a Poisson shot noise in which $a_{\text{signal}} = 1.1$ nA, 2nd column: Background current, $I_{\text{noise}}(t)$, a Poisson shot noise, 3rd column: Raster plots of 30 trials. *Bottom* Post-stimulus time histogram (PSTH). The amplitude of $h_{\text{noise}}(t)$, a_{noise}, was set at 0.1 nA in (**a**), 0.15 nA in (**b**), and 0.3 nA in (**c**)

Figure 4 shows the inter-spike interval (ISI) histograms generated from 100 (10 samples times 10 trials) spike trains in which the random sub-threshold synaptic current $I_{\text{signal}_C}(t)$ with an intensity of 5 s^{-1} and $a_{\text{signal}} = 1.1$ nA was applied to the distal point in the presence of the background noise, $I_{\text{noise}}(t)$, with an intensity of 100 s^{-1}. The amplitude of the background noise was set at 0.1 nA in (a), 0.15 nA in (b), and 0.25 nA in (c). As the amplitude of background noise increased, longer ISIs disappeared, implying that the background noise itself created unwanted noisy spike firings. These ISI histograms were used for calculating the total entropies, $H_{\text{total}}(T)$ (9).

The mean and standard deviation of the information rate calculated from (8) and (9) as a function of the noise amplitude a_{noise} are shown by the curve "Sub-threshold signal @ C (distal)" in Fig. 5. The information rate reached a maximum value at a noise amplitude of 0.14, thereby displaying SR. These results clearly show that background noise can improve information transmission of sub-threshold input signals in a spiking model of hippocampal CA1 neuron.

Figure 5 shows the information rate as a function of the noise amplitude a_{noise} in which the intensity λ of the homogeneous Poisson shot noise in the input synaptic current was set at 5 s^{-1}. The mean and SD of the information rate estimated from three sample sets for each location are plotted.

3.2 Effect of the input signal location

Previous simulation experiments have shown that the location of the noise source within the neuron does not affect the SR effect but the location of the input signal can modulate or eliminate SR (Stacey and Durand 2000). To determine the effect of the location, the input signal was applied separately in each simulation to proximal (A), medial (B) and distal (C) location within apical tree. Inputs B and C were sub-threshold, while input A was supra-threshold. The information rate reached a maximum value (about 0.35 bits/s) for noise levels of 0.12 and 0.14 when sub-threshold input was applied medially (B) and distally (C), respectively, due to SR. In both cases, the information rate then decreased to value around 0.18 bits/s. However, the information rate for location A started significantly higher (0.75 bits/s) as expected since the signal is supra-threshold but continuously decreased with increasing noise to a baseline level of 0.2 bits/s. Taken together these results show that SR can enhance the information transmission of sub-threshold signals but added noise decreases the information rate of supra-threshold signals.

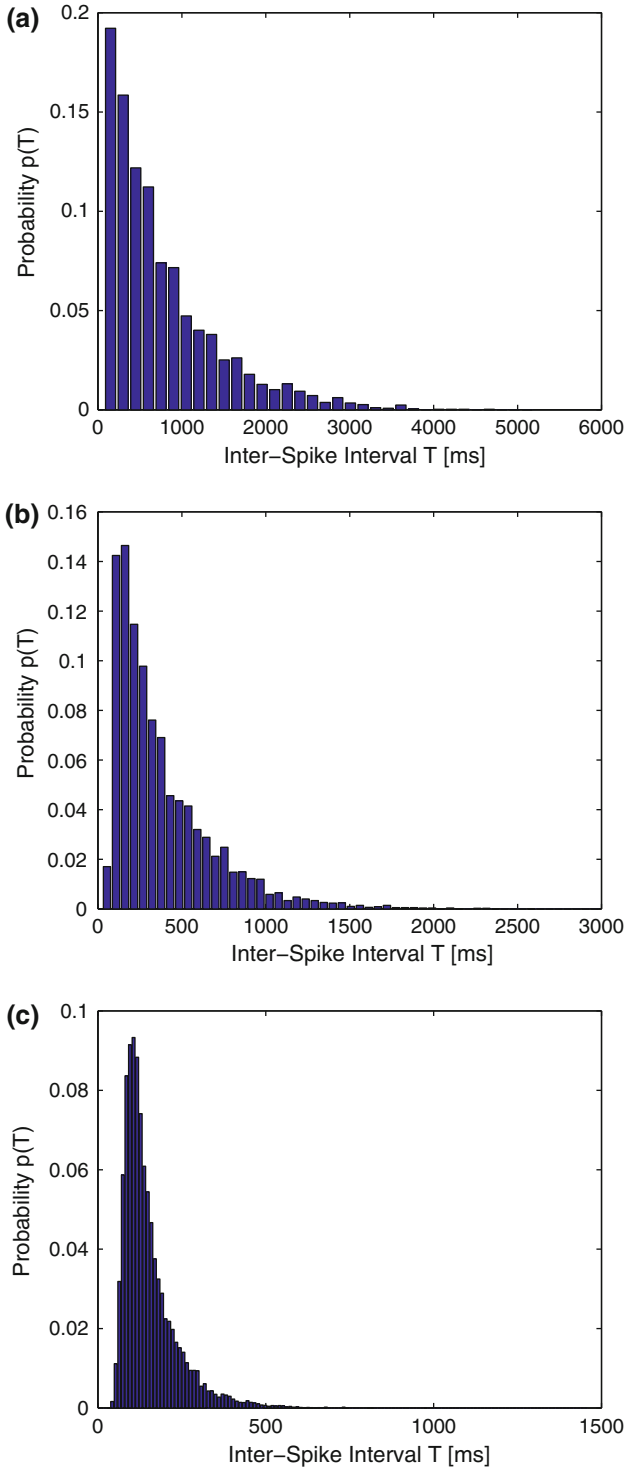

Fig. 4 The inter-spike interval (ISI) histograms generated from 100 (10 samples times 10 trials) spike trains in which the random sub-threshold synaptic current $I_{\text{signal}_C}(t)$ with an intensity of 5 s^{-1} and a_{signal} =1.1 nA was applied to the distal point in the presence of the background noise, $I_{\text{noise}}(t)$, with an intensity of 100 s^{-1}. The amplitude of the background noise was set at 0.1 nA in (**a**), 0.15 nA in (**b**), and 0.25 nA in (**c**). The ISI histograms were used for calculating the total entropies

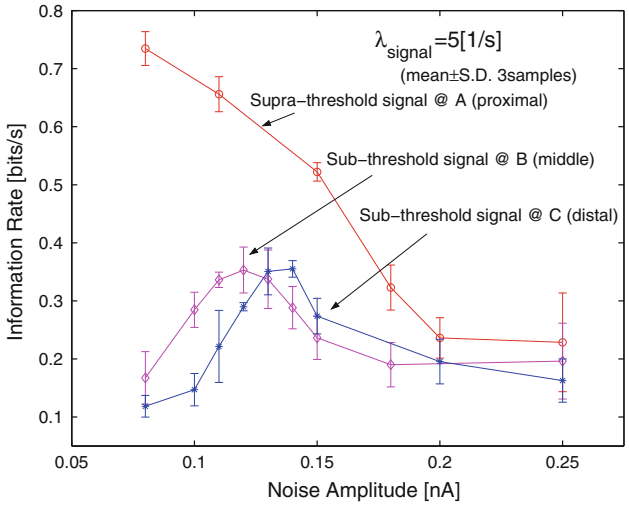

Fig. 5 The information rate as a function of a_{noise} in nA. The signal position was set separately in each simulation at A, B, and C at the intensity λ of 5 s^{-1}. The mean (dots) and SD (bars) of the information rate estimated from three samples were plotted

3.3 Effect of the signal intensity λ of homogeneous Poisson process

The origin of a large component of the noise observed in neurons can be attributed to random release of synaptic vesicles. This release can be modeled by a homogeneous Poisson process, and the post-synaptic current can be modeled by a filtered Poisson process (Poisson shot noise). A Poisson shot noise is characterized by its amplitude a_{noise} and mean frequency (or intensity) λ between 0 and 8 (Abenavoli et al. 2002). We therefore investigated the role of the mean frequency on SR by estimating the information rate as a function of a_{noise} for various values of λ. The input signal was placed at location C.

Figure 6 shows the information rate as a function of a_{noise} with intensity λ of the homogeneous Poisson process set at 2.5, 5, 8, and 10. With λ set at 2.5 and 5, SR was observed since the information rate reached a maximum for $a_{\text{noise}} = 0.14(\lambda = 5)$ and $a_{\text{noise}} = 0.17(\lambda = 2.5)$. However, with higher values of λ (8 and 10), the SR was not observed since the input signals were partially supra-threshold. Figure 6 also shows the paradoxical result that the information rate of low amplitude signals can be higher than higher amplitude signals in the presence of added noise.

4 Discussion and conclusion

In this article, we have investigated the information transmission in which a random sub-threshold synaptic current was

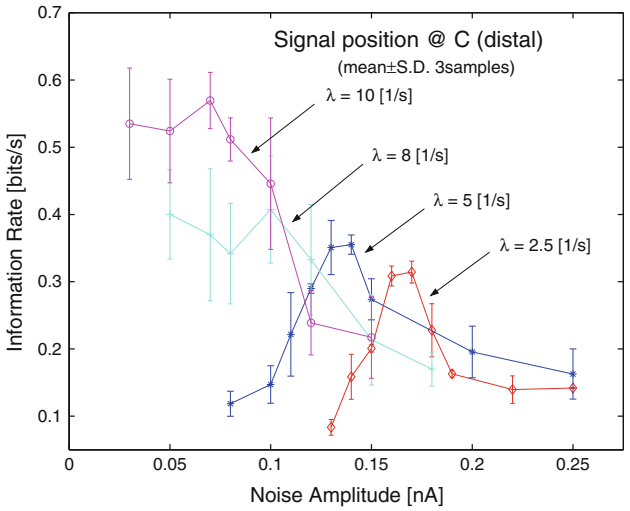

Fig. 6 The information rate as a function of a_{noise} in nA in which the intensity λ of the homogeneous Poisson process in the random synaptic current was set at 2.5, 5, 8, and 10 s^{-1}. The signal position was at C. The mean (dots) and SD (bars) of the information rate estimated from three samples were plotted

presented as stimuli into a proximal, middle, or distal point of the apical dendrite in a hippocampal CA1 neuron model having the soma consisting of one sodium, one calcium, and five potassium channels in the presence of noise. We have shown through computer simulations that at a specific amplitude of the noise, the information rate was found to be maximized due to SR in the cases of sub-threshold stimuli applied to the middle or distal positions on the dendritic tree, i.e., the possibility to encode the random sub-threshold synaptic current into neural spike trains became greater. Although SR was observed in terms of SNR in a biologically realistic neuron model in (Stacey and Durand 2000, 2001), we note that those results based on SNR do not tell us anything about information transmission, information rate, and encoding properties, as explained above. Therefore, the results in this article give an insight into an understanding of the influence of "noise" or fluctuations on information transmission of spikes (action potentials) in a biologically realistic neuron model.

The important issue of investigating the effects of SR on information transmission through computer simulations is to verify that the noise levels are within the physiological range observed in brain slice experiments. Brain slice experiments have shown an intracellular baseline noise variance of 12,000 μV^2 (Stacey and Durand 2000), and Destexhe and Pare (Destexhe and Pare 1999) suggested that the noise variance would increase 100–300 times of the baseline noise variance in active states, i.e., 1.2–3.6 mV^2 (100–300 times of 12,000 μV^2). The variance of the transmembrane potentials, V_m relative to the resting potential, at soma was plotted as a function of the amplitude of the background noise, a_{noise} (see Fig. 2b). The optimal variance of V_m at soma in the case of sub-threshold synaptic currents applied to location C at $\lambda = 5$ s^{-1} was found to be about 1.38 mV^2. The results suggest that the noise levels used in this investigation are within the physiological range, implying the relevance of the computer modeling and simulations.

SR may help explain how distal sub-threshold synaptic currents can be encoded into neural spike trains observed at soma. We have shown that information rate of attenuated distal signals is maximized when background synaptic noise is added to the basal dendrite of CA1 neuron models, even with completely passive dendrites. SR, therefore, explains how CA1 neuron model can improve information transmission if active channels would not exist in the dendrites. Also, SR using synaptic noise may serve to effectively decrease the electrotonic length in neuron model, decreasing dependency on input position under high-noise circumstances (see Fig. 5 (@B, middle; @C, distal)). Further, we have shown the effects of the signal intensity λ on the information transmission when the signal intensity of random sub-threshold synaptic current was set at 2.5, 5, 8, and 10 s^{-1}. It was shown that SR can serve to increase the information transmission of sub-threshold synaptic currents at $\lambda = 2.5$ and 5 s^{-1}, whereas the noise did not help information transmission of supra-threshold synaptic currents at $\lambda = 8$ and 10 s^{-1} (see Fig. 6). These results imply that the "noise" or fluctuations makes it easier to encode sub-threshold synaptic current into neural spike trains within theta-rhythm frequency range (about 4–8 Hz) for the formation of memory (Axmacher et al. 2006).

Therefore, it is concluded that SR can improve information transmission in distal synaptic input with an intensity like the theta-rhythm frequency range in our hippocampal CA1 neuron model. Since SR can clearly improve the signal-to-noise ratio as tested in the rat hippocampal slice in experiments, these computer simulation results suggest that information transmission may also be improved in biological neural networks. Experiments have yet to be carried out to test the predictions of the neuron model.

Appendix

CA1 neuron model

The transmembrane potential $V_m(x,t)$ was calculated by solving the partial differential equation as functions of space x and time t as follows:

$$h^2 \frac{\partial}{\partial x}\left(\frac{1}{R_a(x)}\frac{\partial V_m(x,t)}{\partial x}\right) = C_m(x)\frac{\partial V_m(x,t)}{\partial t} + \frac{V_m(x,t)}{R_m(x)} + I_{\text{ion}}(t)$$

where h denotes an infinitesimal space of x, and $C_m(x)$, $R_m(x)$, and $R_a(x)$ designate the capacitance and resistance

at the compartment and the resistance between the compartments, respectively. The expression discretized at space k and time t was given by

$$\begin{aligned}
&C_m^{[k]}\frac{V_m^{[k]}[t+\Delta t]-V_m^{[k]}[t]}{\Delta t}+\frac{V_m^{[k]}[t]}{R_m^{[k]}}\\
&\quad+I_{\text{ion}}^{[k=\text{soma}]}[t]\delta[k-\text{soma}]\\
&=\frac{V_m^{[k+1]}[t]-V_m^{[k]}[t]}{R_a^{[k+1,k]}}+\frac{V_m^{[k-1]}[t]-V_m^{[k]}[t]}{R_a^{[k,k-1]}}\\
&\quad+\frac{V_m^{[\text{branch}]}[t]-V_m^{[k]}[t]}{R_a^{[\text{branch,k}]}}\delta[k-\text{branch}]
\end{aligned}$$

in which $\delta[\ ]$ denotes Kronecker's delta function. In practical situations, the following formula was solved on the basis of Crank–Nicholson method:

$$\begin{aligned}
&\frac{1}{R_a^{[k-1,k]}}V_m^{[k-1]}[t+\Delta t]\\
&\quad-\left(\frac{1}{R_a^{[k-1,k]}}+\frac{1}{R_a^{[k+1,k]}}+\frac{1}{R_m^{[k]}}+\frac{2C_m^{[k]}}{\Delta t}+\frac{\delta[k-\text{branch}]}{R_a^{[\text{branch,k}]}}\right)\\
&\quad\times V_m^{[k]}[t+\Delta t]+\frac{1}{R_a^{[k+1,k]}}V_m^{[k+1]}[t+\Delta t]\\
&\quad+\frac{\delta[k-\text{branch}]}{R_a^{[\text{branch,k}]}}V_m^{[\text{branch}]}[t+\Delta t]\\
&=-\frac{1}{R_a^{[k-1,k]}}V_m^{[k-1]}[t]\\
&\quad+\left(\frac{1}{R_a^{[k-1,k]}}+\frac{1}{R_a^{[k+1,k]}}+\frac{1}{R_m^{[k]}}+\frac{2C_m^{[k]}}{\Delta t}+\frac{\delta[k-\text{branch}]}{R_a^{[\text{branch},k]}}\right)\\
&\quad\times V_m^{[k]}[t]-\frac{1}{R_a^{[k+1,k]}}V_m^{[k+1]}[t]-\frac{\delta[k-\text{branch}]}{R_a^{[\text{branch},k]}}V_m^{[\text{branch}]}[t]\\
&\quad-I_{\text{ion}}^{[k=\text{soma}]}[t]\delta[k-\text{soma}]
\end{aligned}$$

where the total ion currents are given by

$$\begin{aligned}
I_{\text{ion}}(x,t)=&I_{Na}(t)+I_{Ca}(t)+I_{K_{CT}}(t)+I_{K_{AHP}}(t)\\
&+I_{K_A}(t)+I_{K_M}(t)+I_{K_{DR}}(t)
\end{aligned}$$

Ion conductances at soma

The ion currents, transition rates, conductances, and reversal potentials are described for one sodium, one calcium, and five potassium conductances:

Sodium conductance

$$\begin{aligned}
I_{Na}(t)&=g_{Na}m^3h^1(V_m(\text{soma},t)-E_{Na})\\
\alpha_m&=\frac{-1.74(V_m-11.0)}{e^{(V_m-11.0)/(-12.94)}-1}\\
\beta_m&=\frac{0.06(V_m-5.9)}{e^{(V_m-5.9)/4.47}-1}\\
\alpha_h&=\frac{3.0}{e^{(V_m+80.0)/10.0}}\\
\beta_h&=\frac{12.0}{e^{(V_m-77.0)/(-27.0)}+1}\\
g_{Na}&=150\ \text{mS/cm}^2\\
E_{Na}&=65\text{mV}
\end{aligned}$$

where V_m has units of mV.

Calcium conductance

$$\begin{aligned}
I_{Ca}(t)&=g_{Ca}s^2r^1(V_m(\text{soma},t)-E_{Ca})\\
\alpha_s&=\frac{-0.16(V_m+26.0)}{e^{(V_m+26.0)/(-4.5)}-1}\\
\beta_s&=\frac{0.04(V_m+12.0)}{e^{(V_m+12.0)/10.0}-1}\\
\alpha_r&=\frac{2.0}{e^{(V_m+94.0)/10.0}}\\
\beta_r&=\frac{8.0}{e^{(V_m-68.0)/(-27.0)}+1}\\
g_{Ca}&=10\ \text{mS/cm}^2\\
E_{Ca}&=-30.5\log_{10}\left(\frac{[Ca,1]}{2000}\right)\text{mV}\\
\frac{\text{d}[Ca,1]}{\text{d}t}&=-\left(\frac{[Ca,1]-0.1}{\tau}-\frac{f_1I_{Ca}(t)}{wzFA}\right)
\end{aligned}$$

where w, z, F, and A denote the diffusion thickness (1 μ), the valence of the calcium ion, Faraday's constant, and the area of soma.

Potassium conductance CT (short-duration Ca- and voltage-dependent)

$$\begin{aligned}
I_{K_{CT}}(t)&=g_{CT}c^2d^1(V_m(\text{soma},t)-E_K)\\
\alpha_c&=\frac{-0.0077(V_m+V_{\text{shift}}+103.0)}{e^{(V_m+V_{\text{shift}}+103.0)/(-12.0)}-1}\\
\beta_c&=\frac{1.7}{e^{(V_m+V_{\text{shift}}+237.0)/30.0}}\\
\alpha_d&=\frac{1.0}{e^{(V_m+79.0)/10.0}}\\
\beta_d&=\frac{4.0}{e^{(V_m-82.0)/(-27.0)}+1}\\
g_{CT}&=120\ \text{mS/cm}^2\\
E_K&=-80\text{mV}\\
V_{\text{shift}}&=40\log_{10}([Ca,1]-55)\ \text{mV}
\end{aligned}$$

Potassium conductance AHP (long-duration Ca-dependent)

$$\begin{aligned}
I_{K_{AHP}}(t)&=g_{AHP}q^1(V_m(\text{soma},t)-E_K)\\
\alpha_q&=\frac{0.0048}{e^{(10\log_{10}[Ca,2]-35.0)/(-2.0)}}
\end{aligned}$$

$$\beta_q = \frac{0.012}{e^{(10\log_{10}[Ca,2]+100.0)/(5.0)}}$$

$$g_{AHP} = 3.3\ \text{mS/cm}^2$$
$$E_K = -80\text{mV}$$
$$[Ca, 2] = 0.13\ \mu\text{M}$$

Potassium conductance M (small persistent muscarinic)

$$I_{K_M}(t) = g_M u^2 (V_m(\text{soma}, t) - E_K)$$
$$\alpha_u = \frac{0.016}{e^{(V_m+52.7)/(-23.0)}}$$
$$\beta_u = \frac{0.016}{e^{(V_m+52.7)/(18.8)}}$$
$$g_M = 6.7\ \text{mS/cm}^2$$
$$E_K = -80\text{mV}$$

Potassium conductance A (A-type transient)

$$I_{K_A}(t) = g_A a^1 b^1 (V_m(\text{soma}, t) - E_K)$$
$$\alpha_a = \frac{-0.05(V_m + 20.0)}{e^{(V_m+20.0)/(-15.0)} - 1}$$
$$\beta_a = \frac{0.1(V_m + 10.0)}{e^{(V_m+10.0)/8.0} - 1}$$
$$\alpha_b = \frac{0.00015}{e^{(V_m+18.0)/15.0}}$$
$$\beta_b = \frac{0.06}{e^{(V_m+73.0)/(-12.0)} + 1}$$
$$g_M = 100\ \text{mS/cm}^2$$
$$E_K = -80\text{mV}$$

Potassium conductance DR (delayed rectifier)

$$I_{K_{DR}}(t) = g_{DR} n^4 (V_m(\text{soma}, t) - E_K)$$
$$\alpha_n = \frac{-0.018 V_m}{e^{V_m/(-25.0)} - 1}$$
$$\beta_n = \frac{0.0036(V_m - 10.0)}{e^{(V_m-10.0)/(12.0)} - 1}$$
$$g_{DR} = 6.7\ \text{mS/cm}^2$$
$$E_K = -80\text{mV}$$

References

Abenavoli A, Forti L, Bossi M, Bergamaschi A, Villa A, Malgaroli A (2002) Multimodal quantal release at individual hippocampal synapses: evidence for no lateral inhibition. J Neurosci 22:6336–6346

Axmacher N, Mormann F, Fernandez G, Elger CE, Fell J (2006) Memory formation by neuronal synchronization. Brain Res Rev 52:170–182

Benzi R, Sutera A, Vulpiani A (1981) The mechanism of stochastic resonance. J Phys A 14:L453–457

Brette R, Guigon E (2003) Reliability of spike timing is a general property of spiking model neurons. Neural Comput 15:279–308

Bulsara A, Zador A (1996) Threshold detection of wideband signals: a noise-induced maximum in the mutual information. Phys Rev E 54:R2185–R2188

Bulsara A, Jacobs E, Zhou T, Moss F, Kiss L (1991) Stochastic resonance in a single neuron model: theory and analog simulation. J Theor Biol 152:531–555

Collins J, Imhoff T, Grigg T (1996) Noise-enhanced information transmission in rat SA1 cutaneous mechanoreceptors via aperiodic stochastic resonance. J Neurophysiol 76:642–645

Cook EP, Johnston D (1997) Active dendrites reduce location-dependent variability of synaptic input trains. J Neurophysiol 78:2116–2128

Cox DR, Lewis PAW (1966) The statistical analysis of series of events. Methuen, London

Dayan P, Abbott LF (2001) Theoretical neuroscience: computational and mathematical modeling of neural systems. The MIT Press, Cambridge, MA

Deco G, Schumann B (1997) Stochastic resonance in the mutual information between input and output spike trains of noisy central neurons. Phys D 117:276–282

de Ruyter van Steveninck RR, Lewen GD, Strong SP, Koberle R, Bialek W (1997) Reproducibility and variability in neural spike trains. Science 275(5307):1805–1808

Destexhe A, Pare D (1999) Impact of network activity on the integrative properties of neocortical pyramidal neurons in vivo. J Neurophysiol 81:1531–1547

Destexhe A, Rudolph M, Pare D (2003) The high-conductance state of neocortical neurons in vivo. Nat Rev 4:739–751

Douglass J, Wilkins L, Pantazelou E, Moss F (1993) Noise enhancement of information transfer in crayfish mechanoreceptors by stochastic resonance. Nature 365:337–340

Gammaitoni L, Hanggi P, Jung P, Marchesoni F (1998) Stochastic resonance. Rev Mod Phys 70:223–287

Kish LB, Harmer GP, Abbott D (2001) Information transfer rate of neurons: stochastic resonance of Shannonś information capacity. Fluctuation Noise Lett 1:L13–L19

Magee J, Johnston D (1995) Synaptic activation of voltage-gated channels in the dendrites of hippocampal pyramidal neurons. Science 268:301–304

Moss F (2000) Stochastic resonance: looking forward. In: Walleczek J (ed) Self-organized biological dynamics & nonlinear control. Cambridge University Press, Cambridge, pp 236–256

Moss F, Pierson D, O'Gorman D (1994) Stochastic resonance: tutorial and update. Int J Bifurc Chaos 6:1383–1397

Moss F, Ward LM, Sannita WG (2004) Stochastic resonance and sensory information processing: a tutorial and review of application. Clin Neurophys 115:267–281

Nicolis C (1982) Stochastic aspects of climatic transitions—response to periodic forcing. Tellus 34:1–9

Rieke F, Warland D, de Ruyter van Steveninck RR, Bialek W (1997) Spikes: exploring the neural code. The MIT Press, Cambridge, MA

Scott DW (1979) On optimal and data-based histograms. Biometrika 66:605–610

Shannon CE (1949) Communication in the presence of noise. Proc IRE 37:10–21

Simonotto E, Riani M, Seife C, Roberts M, Twitty J, Moss F (1997) Visual perception of stochastic resonance. Phys Rev Lett 78:1186–1189

Snyder DL, Miller MI (1991) Random point processes in time and space, 2nd edn. Springer-Verlag, New York

Spruston N, Jaffe DB, Williams SH, Johnston D (1993) Voltage- and space-clamp errors associated with the measurement of electrically remote synaptic events. J Neurophysiol 70:781–802

Stacey WC, Durand DM (2000) Stochastic resonance improves signal detection in hippocampal CA1 neurons. J Neurophysiol 83:1394–1402

Stacey WC, Durand DM (2001) Synaptic noise improves detection of subthreshold signals in hippocampal CA1 neurons. J Neurophysiol 86:1104–1112

Stacey WC, Durand DM (2002) Noise and coupling affect signal detection and bursting in a simulated physiological neural network. J Neurophysiol 88:2598–2611

Stein RB, Gossen ER, Jones KE (2005) Neuronal variability: noise or part of the signal?. Nat Rev 6:389–397

Traub RD (1982) Simulation of intrinsic bursting in CA3 hippocampal neurons. Neuroscience 7:1233–1242

Warman EN, Durand DM (1994) Reconstruction of hippocampal CA1 pyramidal cell electrophysiology by computer simulation. J Neurophysiol 83:2192–2208

Zador A (1998) mpact of synaptic unreliability on the information transmitted by spiking neurons. J Neurophysiol 79:1219–1229